Determining small refractive index contrast in chalcogenide-glass pairs at mid-infrared wavelengths

Y. FANG,[1] D. FURNISS,[1] D. JAYASURIYA,[1,2] H. PARNELL,[1,3] R. CRANE,[1] Z. Q. TANG,[1] E. BARNEY,[1] C. L. CANEDY,[4] C. S. KIM,[4] M. KIM,[5] C. D. MERRITT,[4] W. W. BEWLEY,[4] I. VURGAFTMAN,[4] J. R. MEYER,[4] A. B. SEDDON,[1] AND T. M. BENSON[1,*]

[1]*Mid-Infrared Photonics Group, George Green Institute for Electromagnetics Research, Faculty of Engineering, University of Nottingham, University Park, NG7 2RD Nottingham, UK*
[2]*Now at ThorLabs, 1 St. Thomas Place, Ely, CB7 4EX, UK*
[3]*Now at Granta Design Ltd. (Materials Intelligence), Rustat House, 62, Clifton Rd., Cambridge CB1 7EG, UK*
[4]*Code 5613, Naval Research Laboratory, Washington, DC 20375, USA*
[5]*KeyW Corporation, Hanover, MD 21076, USA*
[*]*Trevor.Benson@nottingham.ac.uk*

Abstract: A two-composition thin film ($Ge_{20}Sb_{10}Se_{70}$/$Ge_{20}Sb_{10}Se_{67}S_3$ atomic % core/cladding glasses) was fabricated using a hot-fibre-pressing technique in which both glasses follow the same post-fibre processing. A simple approach is proposed that uses normal incidence transmission spectra to determine their refractive index contrast over the wavelength range from 2 to 25 μm with an error of less than ± 0.002. Using an improved Swanepoel method, the calculated numerical aperture of these two compositions was within ± 0.011 of that obtained from prism minimum deviation measurements. Results show that introducing 3 atomic % S into the Ge-Sb-Se glass system lowered the refractive index and blue-shifted the visible optical bandgap, the far-infrared fundamental vibrational absorption bands and the zero-dispersion wavelength.

1. Introduction

The chalcogenide-glasses, which are based on one or more Group 16 elements of the Periodic Table: sulfur (S), selenium (Se) or tellurium (Te), are promising materials for mid-infrared (MIR) applications [1,2]. With additions of germanium (Ge), antimony (Sb) or arsenic (As) [3,4], chalcogenide-glasses offer a wide range of glass compositions, glass-stability, robustness, high refractive index, high optical non-linearity, low phonon energy and mid-infrared (MIR) transparency, as well as good chemical durability [5–7]. With these properties, chalcogenide-glasses are attractive for use in planar photonic integrated circuits [8–10], supercontinuum generation [11] and amplifiers [12–15] for the MIR. Moreover, chalcogenide-glasses can also be drawn into optical fibres for MIR remote sensing applications [16–18]. Optical fibres based on Ge-Sb-Se are attractive for bio-sensing because of the lowered toxicity, on replacing As with Sb, and transmission to longer wavelengths to span the "fingerprint" absorption region of organic biomolecules. Ge-Sb-Se fibres are good candidates for bio- and chemical-sensing, again due to their robustness, good thermal, mechanical and chemical properties, and high transparency across the wavelength range from 2 to 16 μm [19–22]. Although many studies have focused on the characterization of chalcogenide-glasses, the refractive index dispersion, and refractive index

contrast, of the optical fibres, two key parameters in supercontinuum generation and step-index fibre design, have been less frequently investigated.

In this work, two chalcogenide-glass compositions, Ge-Sb-Se ($Ge_{20}Sb_{10}Se_{70}$ (atomic % (at. %)) and Ge-Sb-Se-S ($Ge_{20}Sb_{10}Se_{67}S_3$ at. %), are studied. These were selected as the core and cladding glasses, respectively, of a low NA (numerical aperture) step-index fibre (SIF) for mid-infrared bio- and chemical-sensing [23].

Refractive index dispersion is one of the critical parameters which influences the design of optical components. Techniques commonly used for refractive index measurement include the modelling of transmission or reflection spectroscopic data [24], spectroscopic ellipsometry [25,26], prism coupling [27], grating coupling [28], and measurement of the minimum deviation angle of light passing through a prism [29]. Several of these techniques require intensive sample preparation, as well as being time consuming and costly to conduct. More importantly it has, until recently, been difficult to apply some of these techniques to the MIR spectral region because of the paucity of suitable beam sources [27].

Nowadays, the most common way to measure the refractive index dispersion and NA is by spectroscopic ellipsometry. In [30], we reported the continuous linear refractive index dispersion at ambient temperature, obtained by means of spectroscopic ellipsometry, of two bulk chalcogenide-glasses, As-Se and Ge-As-Se, over the 0.4 μm - 33 μm wavelength range. A two-term Sellmeier equation, with one resonant visible-region absorption and one resonant MIR absorption, was determined as sufficient and appropriate for fitting the refractive index dispersion over the wavelength range for which the extinction coefficient was less than 0.0005. The fitting accuracy was better than 0.1%. Nevertheless, the accuracy in measuring the refractive index by means of spectroscopic ellipsometry is inherently limited by surface effects [31], as a thin contamination layer, oxide layer, or small defects on the surface can potentially alter the measured optical constants. With the advantages of time-saving sample preparation, wide and continuous wavelength measurement region and insensitivity to small defects on the surface, an improved Swanepoel method [32], which upgraded the original Swanepoel method [24] by changing the dispersive equation from a Cauchy to a Sellmeier equation to extend the technique into the MIR region, can be used to determine the refractive index dispersion of chalcogenide-glasses to an accuracy of better than 0.4% [32].

Here, a two-composition chalcogenide-glass thin film (Ge-Sb-Se ($Ge_{20}Sb_{10}Se_{70}$ (atomic % (at. %)) and Ge-Sb-Se-S ($Ge_{20}Sb_{10}Se_{67}S_3$ at. %)) was fabricated to compare the refractive index contrast of two glass compositions with virtually the same thermal history and post-fibre processing. A fast and simple method was developed to compare the refractive index contrast of the two compositions comprising the thin film by using the normal-incidence transmission spectra only. To directly determine the refractive index data, as well as the thickness of the thin film, the improved Swanepoel method was applied with an accuracy of better than 0.4%. In the low NA optical fibre design, 3 at. % S was substituted for Se to give the Ge-Sb-Se-S cladding composition. The effect of this 3 at. % S substitution on the refractive index, NIR (near-infrared) optical bandgap, MIR fundamental absorption and zero dispersion wavelength are reported here.

The remainder of the Paper is organised in the following way: in Section 2, the core and cladding glass melts of Ge-Sb-Se, Ge-Sb-Se-S, respectively, are introduced. This section also presents the preparation of the two-composition thin film. Section 3 discusses the experimental setup. Section 4 presents a fast, simple method to compare the refractive index contrast [33] between the two compositions in the two-composition thin film. To directly obtain the refractive indices, and hence the refractive index contrast of these two compositions, the improved Swanepoel method was applied in this Section. Section 4 also presents the NA and dispersion data of the two compositions. Additionally, the effects of substituting 3 atomic % S for Se in Ge-Sb-Se are discussed. Finally, the important conclusions drawn from the study are highlighted in Section 5.

2.   Sample preparation

2.1.   *Glass melting*

The $Ge_{20}Sb_{10}Se_{70}$ and $Ge_{20}Sb_{10}Se_{67}S_3$ at. % glass compositions (as-batched) studied here were prepared by the traditional melt-quench technique and have been shown to yield glass compositions close to that as-batched [23]. The Se (99.999%; Materion, ABSCO Materials, Suffolk, UK), Sb (99.9999%, Cerac, ABSCO Materials) and S (99.999% Materion, ABSCO Materials) elemental precursors were purified *via* a vacuum bake-out procedure to try to remove oxide, hydride and water-based impurities. Ge (5 N purity, Materion) was untreated, as elemental Ge and Ge-oxides have low, and similar vapour pressures, even at high temperature (Parnell *et al.* 2018). Before batching the elements, the silica-glass ampoule (MultiLab, UK, < 1 ppm [-O-H]) used for the chalcogenide-glass melt-containment was etched using 40% $^v/_v$ hydrofluoric acid (HF), rinsed with deionised water and dried under N_2 (99.998% BOC, white-spot) under rotary pump evacuation ($\sim 10^3$ Pa). The ampoule was then air-baked and subsequently vacuum baked ($\sim 10^{-3}$ Pa), each at 1000 °C for 6 h, in the same vertical furnace (TF105/4.5/IZF, Instron) to drive off carbon-based impurities and physisorbed, and chemisorbed, water, respectively, from the inside surface of the ampoule. As-supplied Ge (99.999%, Materion) was batched into the prepared ampoule, along with the purified Sb, Se and S, under a N_2 atmosphere (99.998% BOC, white-spot) in an MBraun glove-box ($\leq$ 0.1 ppm H_2O and $\leq$ 0.1 ppm O_2). After batching, the ampoule was sealed under vacuum (10^{-3} Pa) using an oxy-propane (BOC gas) torch (Jencons, Junior Jet 7, East Grinstead, UK) and placed in a rocking furnace to melt and homogenise the chalcogenide-glass, at $\sim$ 900 °C / 24 h. After cooling to 700 °C, and vertical refining and fining, the ampoule was removed from the furnace and quenched. The chalcogenide-glass was annealed *in situ*, inside the ampoule, at the DSC-measured (differential scanning calorimetric [34]) onset-T_g (glass transition) for 0.5 h, before cooling down to room temperature.

   Both the thin film (Section 2.2) and prism refractive index samples were made from the same glass-melt. Prisms were ground and polished in-house to a 1 μm finish, with the glass piece supported on a jig, and to have opposite faces supporting a nominal 20 ° prism apex angle (subsequently measured to be 20 ° 09' for Ge-Sb-Se and 20 ° 09' for Ge-Sb-Se-S with an error of ± 1').

2.2.   *Thin film sample preparation*

The two-composition ($Ge_{20}Sb_{10}Se_{70}$ (i.e. Ge-Sb-Se) and $Ge_{20}Sb_{10}Se_{67}S_3$ (i.e. Ge-Sb-Se-S) at. %) thin films were prepared by a hot-pressing technique described in [8,10,29,32].

   The as-annealed preforms ($\sim$10 mm diameter and $\sim$ 70 mm length) of Ge-Sb-Se and Ge-Sb-Se-S, prepared as in section 2.1, were each drawn into unstructured (i.e. single composition) optical fibre on a customised Heathway draw-tower, housed in a 10,000 - Class clean-room. The fibres were drawn at a viscosity of around $10^{4.5}$ Pa.s under a N_2 flow (99.998% BOC white-spot). The final fibre diameter was 250 ± 10 μm. The outer surface of the fibres was shiny and no defects could be seen by the naked eye. Short sections of the Ge-Sb-Se and Ge-Sb-Se-S fibres, each of 250 ± 10 μm diameter and 20 mm length, were obtained by cleaving. The fibre samples were etched in propylamine (Sigma-Aldrich 99 mol.%) for 30 min at room temperature under atmospheric pressure and then cleaned using isopropanol (IPA, HPLC grade, Fisher Chemical) and optical lens tissue. The Ge-Sb-Se and Ge-Sb-Se-S fibres were then placed, aligned axially, on a tungsten carbide plate (800 mm diameter, of flatness ± 0.08 μm and of surface finish ± 0.009 μm) that was surrounded by a 25 μm thick stainless-steel shim (Hollinbrow Ltd., UK) and then covered by a second tungsten carbide plate. The distance between the two fibres: Ge-Sb-Se and Ge-Sb-Se-S was, from experience, set at 1 mm to allow the glass supercooled-melts to spread until touching during pressing but not to move into each other. The fibre samples were hot-pressed under vacuum (10^{-4} Pa) at 260°C (temperature at which the viscosities of both

glasses were $\sim 10^8$ Pa s [23]) for 12 h with a maximum pressure of 700 N between the two plates. The pressure was removed at the temperature of 260°C. The samples were then cooled down at a low rate (10°C / h) through the T_g region (from 230 to 200°C) and then allowed to cool down naturally, with the equipment, under the vacuum to room temperature. The resulting stand-alone thin film is shown in Fig. 1(a), and this thin film is hitherto termed: 'two-composition (Ge-Sb-Se and Ge-Sb-Se-S) thin film'. The red circle (i) in Fig. 1(a) indicates the SEM-EDX (scanning electron microscope energy dispersive X-ray analysed composition measurement location of the Ge-Sb-Se part in the two-composition thin film, and the circle (ii) in Fig. 1(a) indicates the measurement location of the Ge-Sb-Se-S part. The average thickness at each part of the two-composition thin film was obtained using the improved Swanepoel method [32], and was 27.92 μm for Ge-Sb-Se and 27.96 μm for Ge-Sb-Se-S, with an error of ± 0.02 μm.
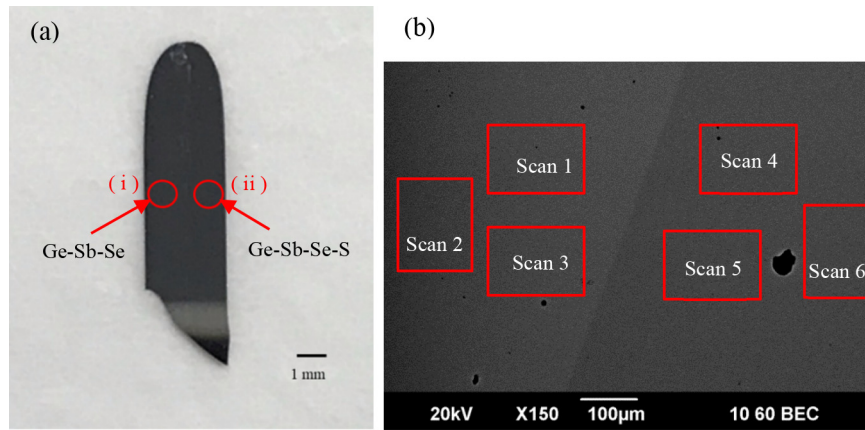

Fig. 1. (a) Photograph of the two-composition thin film comprised of nominal batch $Ge_{20}Sb_{10}Se_{70}$ / $Ge_{20}Sb_{10}Se_{67}S_3$ at. % thin film. The red circles indicate the measurement locations at each part of the thin film; (b) The SEM image of the same two-composition thin film. The contrast shows the interface of the two different materials. The red rectangles indicate the positions of the scans. Scans 1-3 are for $Ge_{20}Sb_{10}Se_{70}$ at. % (measured concentrations in Table 1), and scans 4-6 are for $Ge_{20}Sb_{10}Se_{67}S_3$ at. % (measured concentrations in Table 1).

A JEOL 6490LV SEM fitted with a X-Max 80 Oxford Instruments EDX detector was used to obtain the exact compositions of both Ge-Sb-Se and Ge-Sb-Se-S parts of the as-prepared two-composition thin film. The image of the two-composition thin film is shown in Fig. 1(b). Three scans near the measurement locations at each side on the two-composition thin film (see Fig. 1(b)) were performed. The composition results obtained from the SEM-EDX analysis are shown in Table 1. As shown in Table 1, it is observed that the Ge-Sb-Se-S part has ~ 3 at. %

Table 1. The compositions at different scan locations (see Fig. 1(b)) on a two-composition thin film obtained using EDX with a SEM. (Key: - means none detected).

Scan location	Ge / at. %	Sb / at. %	Se / at. %	S / at. %
1	20.6	11.7	67.7	-
2	20.3	11.0	68.7	-
3	21.1	11.4	67.5	-
4	20.7	11.4	65.0	2.9
5	21.4	11.3	64.2	3.1
6	20.4	11.3	65.4	2.9

Se less than that in the Ge-Sb-Se part and contains ~ 3 at. % S, which was not found in the Ge-Sb-Se part.

3.   Experimental set-up for refractive index and dispersion measurement

A Globar[TM] source (Bruker), KBr beam splitter (Bruker) and DLaTGSD301 detector (Bruker) were set up in a FTIR (Fourier transform infrared) spectrometer (Bruker IFS 66v/s) to measure the interference, normal-incidence transmission spectra of the two-composition thin films (see section 2.2) in the wavelength range from 1 to 27 µm; 27 µm was the maximum wavelength possible with this set-up in the Bruker FTIR. Due to the low efficiency of the KBr beam splitter and the DLaTGSD301 detector at wavelengths below 2 µm, clear extrema of interference fringes were only obtained over the wavelength range from 2 to 25 µm.

   The stand-alone two-composition (Ge-Sb-Se and Ge-Sb-Se-S) thin film prepared using the hot-pressing technique (section 2.2) was mounted on a home-made rotation stage, which was accurate to ± 0.5 °, installed in the sample compartment of the FTIR spectrometer. In the FTIR spectrometer a 0.651 µm wavelength He-Ne laser beam, intrinsic to the FTIR and used for alignment, indicated the position of the Globar[TM]. The FTIR spectrometer was purged using dry air to remove CO_2 and water. Careful alignment was undertaken to ensure that the axis of rotation of the sample went through the surface of the thin film at the focal point of the He-Ne beam, and that no lateral displacement of the light took place during rotation. The measurement location at each part of the materials in the two-composition thin film is indicated as the red circles in Fig. 2(b). The location of normal-incidence was determined by ensuring that equivalent transmission spectra were obtained after rotation through equal angles in a clockwise and anti-clockwise sense. After obtaining the transmission spectrum at normal incidence, the rotation stage was rotated by an angle of 30° to obtain the transmission spectrum with an incident
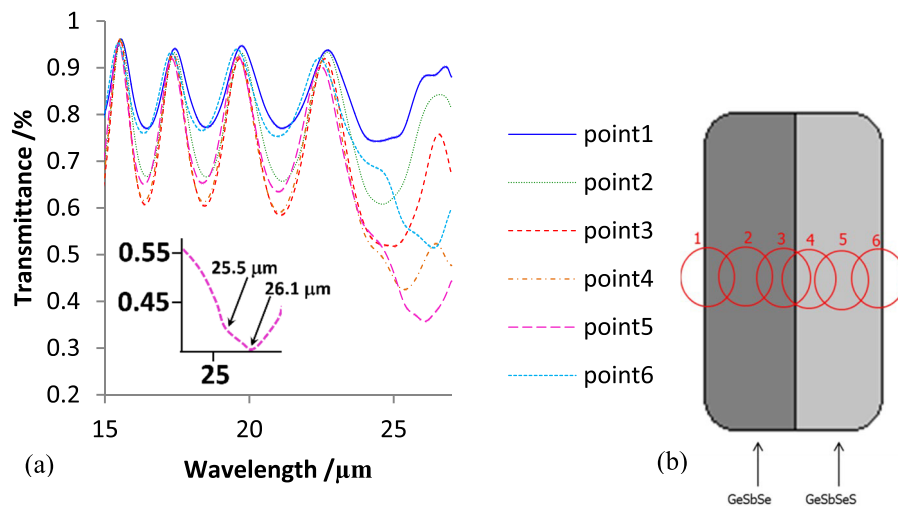

Fig. 2. (a) The transmission spectra at different locations (shown schematically in (b)) of a two-composition (Ge-Sb-Se / Ge-Sb-Se-S) = (core / cladding glasses) thin film. Points 2 and 5 were most representative of the core glass and cladding glass, respectively, without edge or interfacial effects. There are no vibrational absorption bands evident for the spectrum taken at point 2 for the core glass. Yet, in the spectrum taken at point 5 for the cladding glass, two vibrational absorption bands are evident at 25.5 µm (small shoulder) and 26.1 µm (strong band), (as indicated in the inset to (a)); the chemical bond vibrations responsible are identified in the text.

angle of 30°. Then the rotation stage was rotated back to the normal incident position, and was rotated by an angle of 30° in the other direction. The transmission spectrum with an incident angle of −30° was obtained using the FTIR spectroscopy. The transmission spectra with an incident angle of 30° and −30° were required for determining the refractive index and thickness of the thin film using the improved Swanepoel method [32].

Refractive index measurements were also carried out using the minimum deviation method on in-house-prepared, bulk-glass prisms of Ge-Sb-Se and of GeSb-Se-S [29]. Sources used for the prism deviation method were: a 3.1 μm interband cascade laser (ICL) fabricated at NRL, USA, (which emitted > 200 mW cw at 25°C), and a 6.45 μm optical parametric oscillator (OPO) from Chromacity Ltd., Edinburgh, UK.

4. Results and discussion

4.1. Ge-Sb-Se/S glasses: molecular structure

The $Ge_{20}Sb_{10}Se_{70}$ at. % core glass is a non-stoichiometric composition which has excess selenium and is equivalent to: $20GeSe_2$-$5Sb_2Se_3$-$15Se$. This composition has an average coordination number of 2.5 rather than the value of 2.6 found for the stoichiometric composition: $20GeSe_2$-$5Sb_2Se_3$.

Sati *et al.* [35] found that for glasses in the series: $Ge_{40−x}Sb_xSe_{60}$ (x = 8, 12, 15, 18 and 20) with average coordination number < 2.67 (posited as a secondary topological threshold) the structure consists of deformed tetrahedra and pyramids, in which at least one Se atom is substituted by Ge or Sb atoms.

According to Boolchand *et al.* [36], the larger bond strength of ≡(Ge-S)- and =(Sb-S)-, as compared to ≡(Ge-Se)- and =(Sb-Se)-, should result in formation of the former in preference to the latter during glass-melting and quenching.

S is smaller than Se and forms stronger bonds and hence the vibrational frequency, v, of ≡[Ge-S], =[Sb-S] atomic bonds is expected to be higher than that of ≡[Ge-Se]- and = [Sb-Se]-chemical bonds according to the Szigetti equation [37]:

$$v \propto (f/m)^{1/2} \tag{1}$$

where: m is the reduced mass of the two vibrating atoms forming the bond and f is the bond force constant related to chemical bond strength. Therefore, vibrational absorption bands of the S-containing cladding glass are expected at higher frequency compared to the Se-only-containing core glass. Moreover, S is less heavy and less polarisable than Se, so the refractive index of the S-containing cladding glass is expected to be lower than that of the Se-only-containing core glass.

4.2. Analysis of observed MIR vibrational absorption bands

The normal-incidence transmission spectra, spanning the wavelength region 15 to 27 μm and obtained at different spatial regions of the Ge-Sb-Se / Ge-Sb-Se-S two-composition thin film are shown in Fig. 2(a). As the incoming beam shifted from the Ge-Sb-Se part to the Ge-Sb-Se-S part of the thin film, which is from points 1 to 6 in Fig. 2(b), the extrema of each transmission spectrum shifted gradually to shorter wavelength. Since the thickness variation across the thin film was less than 0.01 μm, the shift of the extrema indicated that the Ge-Sb-Se thin film had a higher refractive index than the Ge-Sb-Se-S thin film, as predicted from glass structural considerations (section 4.1).

In Fig. 2(a), points 2 and 5 are anticipated to correspond most closely to the Ge-Sb-Se and Ge-Sb-Se-S core and cladding glass compositions, respectively, because these points are sited in the middle of the corresponding pressed fibre region and are neither near the fibre-edges nor near the interface between the two pressed fibres. The interference transmission spectrum collected at point 5 of the Ge-Sb-Se-S cladding glass shows some obvious absorption dips above 25 μm,

at: 25.5 μm (small shoulder) and 26.1 μm (strong) (both highlighted in the inset to Fig. 2(a)). In contrast, the interference transmission spectrum collected at point 2 of the Ge-Sb-Se core glass exhibits smooth interference fringes only, with no obvious absorption. To understand these spectral changes in the MIR region, the fundamental, overtone and combination vibrational modes of the constituent chemical bonds which may be responsible are considered.

Petit *et al.* [38], in studying the two-glass series: $(1-x)GeS_2-xSb_2S_3$ (with increasing x) and $Ge_{0.23}Sb_yS_{0.77-y}$ (with increasing y), reported stretching vibrational absorption at 26.3 μm of $[GeS_4]$ tetrahedra. Thus, it is proposed that the strong vibrational absorption found at 26.1 μm in the interference transmission spectrum collected at point 5 (Ge-Sb-Se-S cladding glass), shown in the inset to Fig. 2(a), is due to $\equiv[Ge-S]-$ within tetrahedral $[GeSSe_3]$ units in the cladding glass structure. El-Sayed [39] has reported the experimental and theoretical MIR vibrational absorption bands of the glass series: $Ge_{28-x}Sb_xSe_{72}$ at. % with increasing x. The calculated wavelength of a band attributed to fundamental $=[Sb-Se]-$ was 49.8 μm. The small shoulder at 25.5 μm observed here in the interference transmission spectrum of the cladding glass therefore may be assigned as the second overtone of fundamental $=[Sb-Se]-$ vibrational absorption at 49.8 μm in pyramidal units of $[SbSe_3]$ or $[SbSSe_2]$. However, the analogous second overtone of $=[Sb-Se]-$ vibrational absorption in pyramidal $[SbSe_3]$ or $[SbSSe_2]$ units, expected at ~ 20 μm (i.e. at approximately half the wavelength of the fundamental band at 40.49 μm observed for the glass series $Ge_{28-x}Sb_xSe_{72}$ at. % by El-Sayed [39]) was observed neither in the interference transmission spectra of the cladding nor core glasses.

4.3. Simple approach to measure which glass has the larger refractive index in the two-composition (Ge-Sb-Se and Ge-Sb-Se-S) thin film

To design and successfully fabricate small NA, step-index optical fibres, it is crucial that the core and cladding glasses are batched and melted accurately so as to retain a higher refractive index of the core relative to the cladding glass. Glass-distillation purification procedures can inadvertently adversely affect the NA of a fabricated chalcogenide glass SIF, particularly if the NA is small - we suggest particular difficulties in achieving fibre-NA ≤ 0.2. A simple method was developed here to compare the refractive indices of two different glasses in the two-composition thin film by using the normal-incidence transmission spectra only.

The transmission spectra of Ge-Sb-Se and Ge-Sb-Se-S at normal-incidence collected from the two-composition thin film are shown in Fig. 3. The data in Fig. 3 are measured separately from those shown in Fig. 2(a), and the measurement location at each material in the two-composition
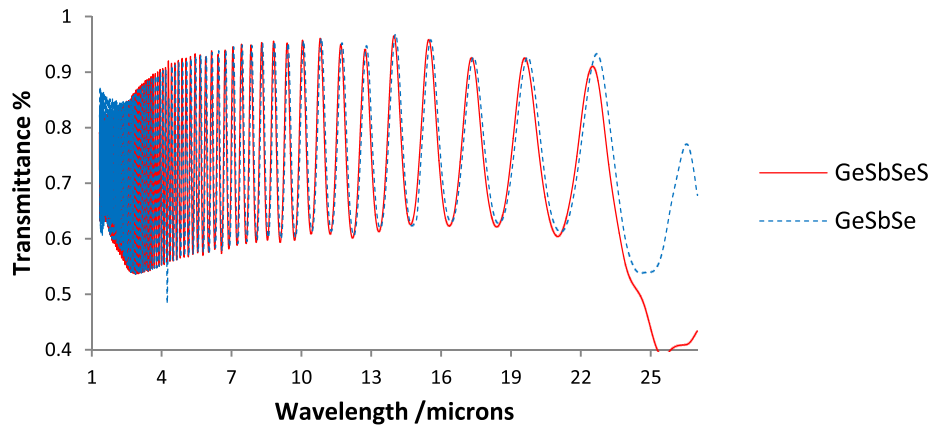

Fig. 3. The transmission spectra of the Ge-Sb-Se (dash curve) and Ge-Sb-Se-S (solid curve) regions of the two-composition thin film at normal incidence.

thin film was indicated as the red circles in Fig. 1(a). For normal-incidence on a thin film with thickness d, the wavelengths of the transmission extrema are given by:

$$2n_0 d = m\lambda_0 \tag{2}$$

where λ_0 is the wavelength at the maxima or minima of the normal-incidence transmission spectrum, n_0 is the refractive index of the material at λ_0, m is the order number which has integer values for the maxima and half-integer values for the minima, and d is the thickness of the thin film. The refractive index contrast of an optical fibre is given by [33]:

$$\Delta = \frac{n_{core}^2 - n_{clad}^2}{2n_{core}^2} = \frac{1}{2}[1 - (\frac{n_{clad}}{n_{core}})^2] \tag{3}$$

where n_{core} is the refractive index in the core and n_{clad} is the refractive index in the cladding. When $n_{clad} > n_{core}$, the refractive index contrast Δ is negative, whereas when $n_{clad} < n_{core}$, Δ is positive. Assuming that the two materials in the two-composition thin film have the same thickness, the refractive index ratio at each extremum for these two materials can be determined by:

$$\frac{n_1}{n_2} = \frac{\lambda_{1m}}{\lambda_{2m}} \tag{4}$$

where m is the order number at each extremum, λ_{1m} is the wavelength at the maxima or minima of the normal-incidence transmission spectrum of the core glass Ge-Sb-Se part, and λ_{2m} is that of the Ge-Sb-Se-S cladding glass. n_1 is the refractive index of core glass Ge-Sb-Se at the wavelength of λ_{1m} and n_2 is the refractive index of cladding glass Ge-Sb-Se-S at λ_{2m}. Substituting Eq. (4) into (3) yields:

$$\Delta = \frac{1}{2}[1 - (\frac{\lambda_{2m}}{\lambda_{1m}})^2] \tag{5}$$

Since these two glasses have a very small refractive index difference, the difference in wavelength at each extremum is small, as shown in Fig. 3. Since the difference between λ_{1m} and λ_{2m} is very small, in the transparency region of interest for most chalcogenide-glasses the difference between $n_1(\lambda_{1m})$ and $n_1(\lambda_{2m})$ is less than 0.0001. Therefore, $n_1(\lambda_{1m})$ and $n_2(\lambda_{2m})$ can be evaluated at approximately the same wavelength. From Fig. 3, λ_{1m} is larger than λ_{2m} which means Δ is positive. Therefore, the Ge-Sb-Se thin film has a higher refractive index than the Ge-Sb-Se-S thin film, as expected (section 4.1).

The refractive index contrast Δ determined by the single measurement at normal-incidence is shown as a function of wavelength in Fig. 4 (blue points) together with a fit to the data points (black solid line). Comparing the two fitted refractive index contrast results obtained at 3.1 and 6.45 μm wavelength, respectively, with those calculated from refractive index measurements for each composition using the minimum deviation method on bulk glass prisms [29], Δ obtained from the normal-incidence only measurement is around 0.0025 lower. This difference is mainly attributed to a thickness difference which must have existed across the two-composition thin film. In this case, the measured thickness variation was 0.04 μm (see section 4.4) which led to a 0.004 change in refractive index. The typical thickness variation of < 0.05 μm leads to an error of less than ± 0.0020 in determining Δ. This also means that this simple method can only correctly determine which glass has the larger refractive index when the refractive index difference between the two glasses in the two-composition thin film is > 0.005.

4.4.   Determining the refractive indices of Ge-Sb-Se and Ge-Sb-Se-S glasses in the two-composition thin film

In most cases, a very small thickness difference (less than 0.05 μm) existed across the 2-composition thin film sample; as noted in section 4.3 this would have caused some error in
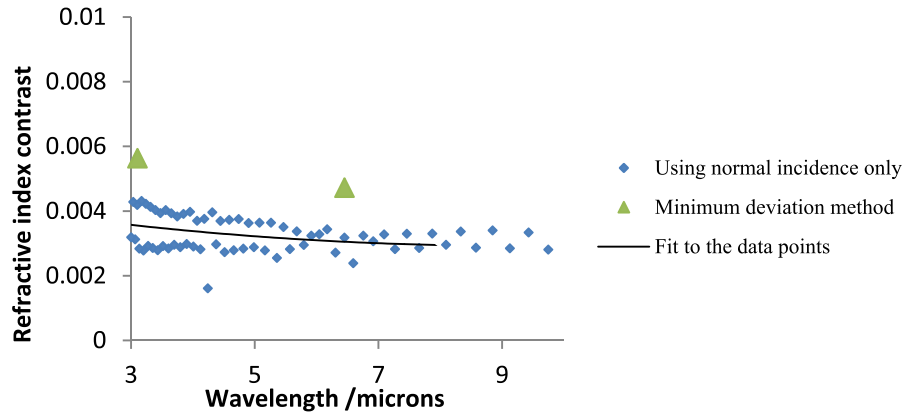
Fig. 4. The refractive index contrasts of the two-composition thin film: Ge-Sb-Se and Ge-Sb-Se-S, determined by a single measurement at normal-incidence and calculated after using the prism minimum deviation method to measure the refractive index of a prism of each composition with sources at 3.1 and 6.45 μm wavelength; all measurements were at ambient temperature.

determining the refractive index contrast. In order to determine the thickness of each part of the two-composition thin film, and to determine the absolute value of the refractive index contrast between the Ge-Sb-Se core glass and Ge-Sb-Se-S cladding glass thin films, the improved Swanepoel method described in [32] was applied.

In [32], the original Swanepoel method [24] was improved and extended into the MIR spectral region by using a two-term Sellmeier model instead of the Cauchy model as the dispersive equation. The Sellmeier relation is defined as:

$$n^2(\lambda) = A_0 + \sum_{n=1}^{N} \frac{A_n \lambda^2}{\lambda^2 - a_n^2} \tag{6}$$

where A_0 and A_n are dimensionless coefficients, N is the number of Sellmeier coefficients (here 2), a_n indicates the N material resonant absorption wavelengths assumed in the model, and λ is the wavelength in free space.

The Sellmeier equations of Ge-Sb-Se and Ge-Sb-Se-S from the improved Swanepoel method were obtained as:

$$n^2 = 5.469 + \frac{1.006\lambda^2}{\lambda^2 - 0.6472^2} + \frac{1.189\lambda^2}{\lambda^2 - 40.82^2} \quad \text{for Ge}_{20}\text{Sb}_{10}\text{Se}_{70} \text{ core.} \tag{7}$$

$$n^2 = 4.956 + \frac{1.458\lambda^2}{\lambda^2 - 0.5022^2} + \frac{0.8864\lambda^2}{\lambda^2 - 35.97^2} \quad \text{for Ge}_{20}\text{Sb}_{10}\text{Se}_{67}\text{S}_3 \text{ cladding.} \tag{8}$$

with correlation coefficient: $R^2 = 0.9976$ for Ge-Sb-Se and $R^2 = 0.9991$ for Ge-Sb-Se-S.

In our previous study of a Sellmeier refractive index model fit to $As_{40}Se_{60}$ at. % ellipsometry data [30], several different sets of Sellmeier coefficients could be obtained, depending on the choice of the a_n parameters in the Sellmeier fit. We believe it is important that the two-term Sellmeier model lends itself to a physical interpretation, as this could open the way to use of the model as a predictive tool. We previously proposed that the a_1 coefficient in the two-term Sellmeier equation be linked to the optical bandgap, while a_2 is associated with the highest energy, vibrational fundamental absorption band due to chemical bond vibration of the glass matrix.

From Eqs. (7) and (8), the a_1 coefficient of Ge-Sb-Se-S (0.5022 μm) is a shorter wavelength than that of Ge-Sb-Se (0.64720 μm), which is in agreement with the hypothesis that introducing S into the Ge-Sb-Se glass system shifts the optical bandgap to shorter wavelength.

The a_2 coefficient of the $Ge_{20}Sb_{10}Se_{70}$ at. % core glass, which is 40.82 μm in Eq. (7), is in good agreement with a literature value of 40.49 μm for MIR vibrational absorption attributed to = [Sb-Se]- in [SbSe$_3$] pyramids in a $Ge_{20}Sb_8Se_{72}$ at. % glass, observed by El-Sayed [39] when studying the glass series $Ge_{28-x}Sb_xSe_{72}$ at. %, with increasing x. For the Ge-Sb-Se core glass here, the a_2 coefficient of the $Ge_{20}Sb_{10}Se_{70}$ at. % core glass of 40.82 μm is therefore also assigned to vibrational absorption due to = [Sb-Se]- in [SbSe$_3$] pyramids.

The a_2 coefficient of the $Ge_{20}Sb_{10}Se_{67}S_3$ at. % cladding glass, which is 35.97 μm in Eq. (8), appears to be reasonably matched in wavelength to the vibrational absorption at 34.5 μm observed by Petit *et al.* [38] in MIR spectra of the two-glass series: $(1-x)GeS_2-xSb_2S_3$ and $Ge_{0.23}Sb_yS_{0.77-y}$; they found that this absorption band tended to broaden and intensify to cover the range 27.8 to 38.5 μm as Sb and/or Sb$_2$Se$_3$ was increased. Petit *et al.* [38] attributed this band to vibrational absorption of [SbS$_3$] pyramidal units. The a_2 coefficient (35.97 μm) of the Sellmeier model for the Ge-Sb-Se-S cladding glass is therefore assigned as = [Sb-S]- vibrational absorption within [SbSSe] pyramidal units in the Ge-Sb-Se-S cladding glass.

It is interesting to note that the fundamental vibrational absorption of antimony chalcogenide (=[Sb-Se] and = [Sb-S]-) chemical bonding controls the value of the a_2 coefficient in the Sellmeier modelling rather than the vibrational absorption of the Ge bonding analogues. The phonon energy of the Sb bonding is at lower energy due to the heavier relative atomic mass of Sb (121.76) compared to Ge (72.64), and weaker chemical bonding of Sb. Note that the a_2 coefficient of the Ge-Sb-Se-S cladding glass is at shorter wavelength than a_2 of the Ge-Sb-Se core glass, which is in agreement with the observation that introducing S into the Ge-Sb-Se glass system will tend to form tetrahedral [Ge(S)$_x$(Se)$_{4-x}$] and pyramidal [Sb(S)$_y$(Se)$_{3-y}$] structural units (see section 4.1), tending to a blue shift in the associated vibrational absorption bands. Of course, accurate positions of the MIR fundamental vibrational absorption bands due to the chalcogenide-glass matrix chemical bonds beyond 25 μm can be determined experimentally by using a MIR detector with a wider wavelength range, which was not available to us at that time.

Figure 5 shows the refractive indices of the Ge-Sb-Se and Ge-Sb-Se-S core and cladding glasses, respectively, obtained for the two-composition thin film from the improved Swanepoel method. For comparison purposes, single-glass Ge-Sb-Se and Ge-Sb-Se-S thin films were also prepared from glass samples from the same glass-melting as for the two-composition thin films, by means of the hot-pressing technique, and each thin film underwent a tailored annealing dwell at its onset-Tg (from DSC [34]) for 1 h while cooling. From Fig. 5, it is found that the error between the results from the two-composition thin film and those from the well-annealed single thin films is less than 0.12% over the wavelength range from 3 to 25 μm.

The refractive indices of the Ge-Sb-Se core glass and Ge-Sb-Se-S cladding glass from the two-composition thin film and single-glass thin films at wavelengths of: 3.1, 5, 6.45, 10 and 15 μm, are shown in Table 2, as well as the results from minimum deviation measurements on polished prisms [29] at wavelengths of 3.1 and 6.45 μm. The minimum deviation prism method in our laboratory can determine the refractive indices of bulk chalcogenide-glasses with a standard deviation of precision of < 0.001 [29]. If we take the prism minimum deviation values as our benchmark value (arbitrarily), then a 0.2% error between the thin film measurements and prism measurements was observed. This difference might be attributable to the different thermal history (fictive temperature) of the thin film and prisms; a glass melt has been quenched and annealed prior to grinding and polishing a prism at room temperature, whereas a thin film's most recent thermal history (which will have eradicated any prior history due to fibre drawing etc.) was the hot-pressing thermal schedule which concluded with an annealing step. It is important to note that neither of these thermal histories reflects the thermal history of a chalcogenide glass SIF
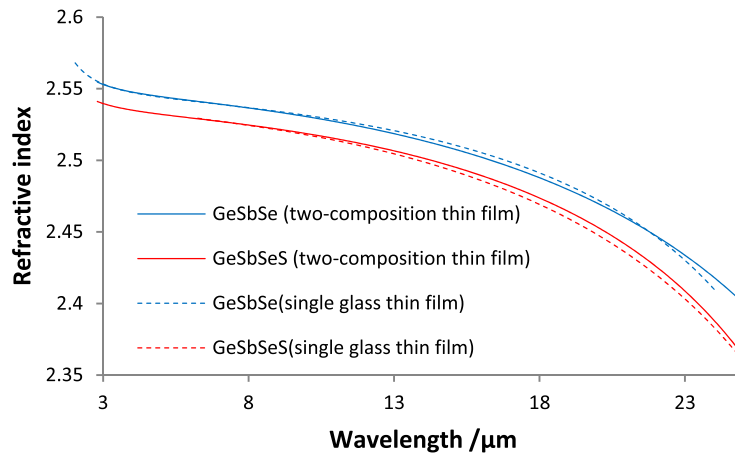
Fig. 5. The refractive indices of the core glass composition Ge-Sb-Se and cladding glass composition Ge-Sb-Se-S determined by applying the improved Swanepoel method [32] to the two-composition hot-pressed thin film and to single-glass thin films of each composition.

or unstructured fibre, taken directly from the draw tower, unless the drawn fibre is subsequently annealed.

Table 2. Refractive indices of the Ge-Sb-Se and Ge-Sb-Se-S glasses at five wavelengths, as obtained by applying the inproved Swanepoel method [32] to both the two-composition hot-pressed thin film and individual glass thin films, and also from minimum deviation measurements on prisms at wavelengths of 3.1 and 6.45 µm.

Wavelength Sample measured	3.1 µm	5 µm	6.45 µm	10 µm	15 µm
Ge-Sb-Se (two-composition hot-pressed thin film)	2.552	2.544	2.541	2.530	2.508
Ge-Sb-Se (single glass hot-pressed thin film)	2.553	2.544	2.542	2.531	2.511
Ge-Sb-Se-S (two-composition hot-pressed thin film)	2.539	2.532	2.529	2.519	2.496
Ge-Sb-Se-S (single glass hot-pressed thin film)	2.540	2.533	2.530	2.518	2.493
Ge-Sb-Se (glass prism)	2.5466	-	2.5354	-	-
Ge-Sb-Se-S (glass prism)	2.5322	-	2.5223	-	-

The refractive index difference of Ge-Sb-Se and Ge-Sb-Se-S prisms was 0.0144 at the wavelength of 3.1 µm, and 0.0131 at 6.45 µm. These values are close to those determined by applying the improved Swanepoel method to the two-composition thin film, which were 0.013 at the wavelength of 3.1 µm and 0.012 at 6.45 µm, respectively. From the refractive indices of the Ge-Sb-Se core glass and the Ge-Sb-Se-S cladding glass found using the improved Swanepoel method for the two-composition thin film, the refractive index contrast can be calculated from Eq. (3); this is shown in Fig. 6.

The thickness of each of the Ge-Sb-Se and Ge-Sb-Se-S pressed films in the two-composition thin sample at the locations indicated in Fig. 1(a), calculated from the improved Swanepoel method, is 27.92 and 27.96 µm, respectively. This observed thickness variation of 0.04 µm leads to a 0.004 change in refractive index. Thus, the simple technique of using the transmission spectra at normal-incidence can determine the refractive contrast when the index difference between two glasses is > 0.005.

To establish the absolute values and thicknesses of each glass, repeated normal-incidence transmission of the two-structural thin film were made and the improved Swanepoel method was applied. Repeated measurements showed that the refractive indices of chalcogenide-glasses
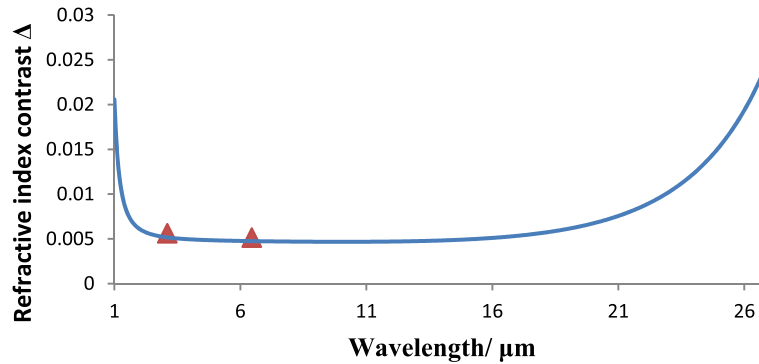
Fig. 6. The refractive index contrast of the two-composition hot-pressed thin film (Ge-Sb-Se core glass and Ge-Sb-Se-S cladding glass) determined using the improved Swanepoel method (solid curve), and prism minimum deviation method (triangles).

were determined by the improved Swanepoel method with a standard deviation of precision less than 0.002 [32]. The refractive index contrast, determined with an error of less than ± 0.0005, compares well with that determined by means of the prism minimum deviation method (assumed bench mark) as shown in Fig. 5. Comparing the results shown in Figs. 4 and 6, it is seen that applying the improved Swanepoel method gives refractive index contrast results in much closer agreement to those obtained from the refractive indices measured separately for each material using the prism minimum deviation method than the simple single normal-incidence measurement approach introduced in section 4.3.

4.5. Numerical aperture and refractive index dispersion

Step-index fibre (SIF) based on the Ge-Sb-Se core and Ge-Sb-Se-S cladding glasses has been successfully fabricated [23]. The numerical aperture (NA) of the SIF composed of the designed glass pair is given by:

$$NA = \sqrt{n_1^2 - n_2^2} \tag{9}$$

where n_1 and n_2 are the refractive indices of the core Ge-Sb-Se glass, and the cladding Ge-Sb-Se-S glass, respectively. As shown in Fig. 7, the NA is around 0.26 over the wavelength range from 3 to 15 μm in the normal dispersion spectral region. The optical bandgap of the Ge-Sb-Se glass is located at a longer wavelength than that of the Ge-Sb-Se-S glass; NA was observed to decrease with increasing wavelength in this shorter-wavelength anomalous dispersion spectral region. Similarly, MIR fundamental vibrational absorption bands of the Ge-Sb-Se-S tend to be located at shorter wavelength compared to analogous bands of the Ge-Sb-Se glass; NA was found to increase gradually in the longer wavelength region (15 to 26 μm) in this longer-wavelength anomalous dispersion spectral region. The difference in *NA* between the thin film measurements and prism measurements was < 0.011. Taking the results from prism measurements as the benchmark (arbitrarily), the error in the NA from the thin film measurements was < 4%.

The material dispersion, *D*, is important data for the design of supercontinuum generation and low dispersion systems; it was calculated here from the standard formula [40]:

$$D = -\frac{\lambda}{c} \left(\frac{d^2 n}{d\lambda^2} \right) \tag{10}$$

where *n* is the refractive index at wavelength; λ is wavelength and *c* is light velocity in a vacuum. For Ge-Sb-Se and Ge-Sb-Se-S, the material dispersion obtained from Eq. (10), using the second derivative of the refractive index given by Eqs. (7) and (8), respectively, is shown in Fig. 8. From
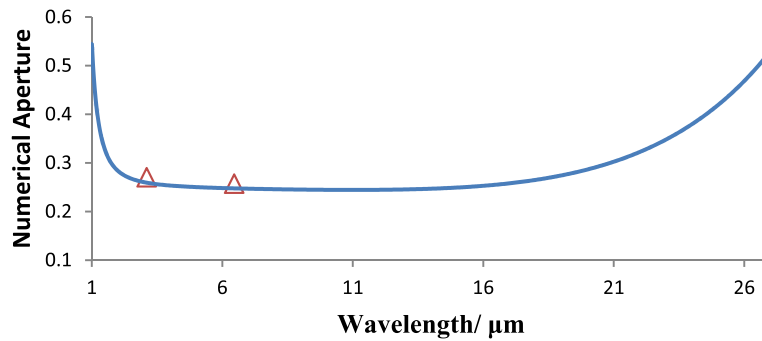
Fig. 7. The NA of step-index fibres based on the Ge-Sb-Se core glass and Ge-Sb-Se-S cladding glass. The blue solid curve is from the two-composition thin film measurements using the improved Swanepoel method; the red triangles are from prism measurements.

Fig. 8, the material zero dispersion wavelengths for Ge-Sb-Se and Ge-Sb-Se-S are at 6.3 and 6.1 μm, respectively. This indicates that for the Ge-Sb-Se-S cladding glass, where 3 at. % S has replaced 3 at. % Se in the Ge-Sb-Se core glass, the zero dispersion wavelength was shifted to a shorter wavelength, by 0.2 μm. This trend is in good agreement with results obtained replacing Se with S in the As-Se glass system, where the zero dispersion wavelength was shifted from 7.2 μm for $As_{40}Se_{60}$ at. % [41] to 4.81 μm for $As_{40}S_{60}$ at. % [42]. It is also important to note that the material dispersion of both Ge-Sb-Se and Ge-Sb-Se-S remains only weakly dependent on wavelength from 3 μm out to 16 μm wavelength, in the normal dispersion spectral region.
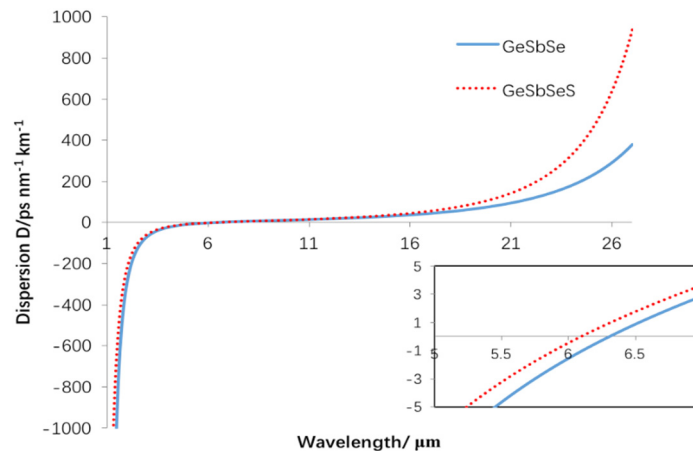

Fig. 8. Material dispersion D calculated from Eq. (10) and the fitted Sellmeier models of the Ge-Sb-Se core glass and Ge-Sb-Se-S cladding glass. Inset: material dispersion close to the material zero dispersion wavelength.

5. Conclusions

A new technique has been developed to determine the small refractive index contrast of two glasses with the same thermal history. The two-composition thin glass film was prepared by a hot-pressing technique. The characteristic interference fringes in the spectral transmission of the two different glasses in the thin film were obtained over the wavelength range from 2 to 27 μm by FTIR spectroscopy; the longer wavelength cut-off was limited by the detector available. Only

using the transmission spectra at normal-incidence, the refractive contrast can be determined over the wavelength range from 2 to 25 μm with an error of less than 0.0020 due to a typically thickness variation of < 0.05 μm of the two-composition thin film. To determine the absolute values of the refractive index and thicknesses of each glass in the two-composition thin film, the improved Swanepoel method was applied. Over the wavelength range 3 to 25 μm, the refractive index can be determined with a standard deviation of precision < 0.002 and the refractive index contrast can be determined with an error of ± 0.0005. The SIF NA was determined from this technique with an error of ± 0.011, compared to the value of SIF NA from the prism minimum deviation method, on samples made from the same glass melts. 3 at. % S replacing Se pro rata in the Ge-Sb-Se glass system (to formulate the cladding glass composition relative to the core glass composition) was shown to blue-shift the NIR optical bandgap and MIR fundamental vibrational absorption bands, lower the refractive index by 0.013 at a wavelength of 3.1 μm and by 0.012 at a wavelength of 6.45 μm, and move the zero dispersion wavelength to shorter wavelength: shifted from 6.3 to 6.1 μm.

References

1. A. B. Seddon, "Chalcogenide glasses: a review of their preparation, properties and applications," J. Non-Cryst. Solids **184**(1), 44–50 (1995).
2. J. S. Sanghera, L. B. Shaw, and I. D. Aggarwal, "Chalcogenide glass-fiber-based mid-IR sources and applications," IEEE J. Sel. Top. Quantum Electron. **15**(1), 114–119 (2009).
3. D. Lezal, "Chalcogenide glasses-survey and progress," J. Optoelectron. Adv. Mater. **5**(1), 23–34 (2003).
4. A. Zakery and S. R. Elliott, "Optical properties and applications of chalcogenide glasses: a review," J. Non-Cryst. Solids **330**(1-3), 1–12 (2003).
5. A. M. Andriesh, "Properties of chalcogenide for optical waveguides," J. Non-Cryst. Solids **77-78**, 1219–1228 (1985).
6. Z. Cimpl and F. Kosek, "Utilization of chalcogenide glasses in infrared optics," J. Non-Cryst. Solids **90**(1-3), 577–579 (1987).
7. I. D. Aggarwal and J. S. Sanghera, "Development and applications of chalcogenide glass optical fibers at NRL," J. Optoelectron. Adv. Mater. **4**(3), 665–678 (2002).
8. A. B. Seddon, W. J. Pan, D. Furniss, C. A. Miller, H. Rowe, D. M. Zhang, E. M. Mcbrearty, Y. Zhang, A. Loni, P. Sewell, and T. M. Benson, "Fine embossing of chalcogenide glasses – a new fabrication route for photonic integrated circuits," J. Non-Cryst. Solids **352**(23-25), 2515–2520 (2006).
9. A. B. Seddon, S. Nabil, N. Abdel-Moneim, L. Zhang, W. J. Pan, D. Furniss, C. J. Mellor, T. Kohoutek, J. Orava, T. Wagner, and T. M. Benson, "Mid-infrared integrated optics: versatile hot embossing of mid-infrared glasses for on-chip planar waveguides for molecular sensing," Opt. Eng. **53**(7), 071824 (2014).
10. N. S. Abdel-Moneim, C. J. Mellor, T. M. Benson, D. Furniss, and A. B. Seddon, "Fabrication of stable, low loss optical loss rib-waveguides via embossing of sputtered chalcogenide glass-film on glass-chip," Opt. Quantum Electron. **47**(2), 351–361 (2015).
11. C. R. Petersen, U. Møller, I. Kubat, B. Zhou, S. Dupont, J. Ramsay, T. Benson, S. Sujecki, N. Abdel-Moneim, Z. Tang, and D. Furniss, "Mid-infrared supercontinuum covering the 1.4-13.3 mum molecular fingerprint region using ultra-high NA chalcogenide step-index fibre," Nat. Photonics **8**(11), 830–834 (2014).
12. R. S. Quimby, L. B. Shaw, J. S. Sanghera, and I. D. Aggarwal, "Modeling of cascade lasing in Dy : chalcogenide glass fiber laser with efficient output at 4.5 μm," IEEE Photonics Technol. Lett. **20**(2), 123–125 (2008).
13. J. Hu, C. R. Menyuk, C. Wei, L. B. Shaw, J. S. Sanghera, and I. D. Aggarwal, "Highly efficient cascaded amplification using Pr[3+]- doped mid-infrared chalcogenide fiber amplifiers," Opt. Lett. **40**(16), 3687–3690 (2015).

14. M. C. Falconi, G. Palma, F. Starecki, V. Nazabal, J. Troles, J. Adam, S. Taccheo, M. Ferrari, and F. Prudenzano, "Dysprosium-doped chalcogenide master oscillator power amplifier (MOPA) for mid-IR Emission," J. Lightwave Technol. **35**(2), 265–273 (2017).

15. M. Shen, D. Furniss, Z. Tang, E. Barny, L. Sojka, S. Sujecki, T. M. Benson, and A. B. Seddon, "Modeling of resonantly pumped mid-infrared Pr^{3+}-doped chalcogenide fiber amplifier with different pumping schemes," Opt. Express **26**(18), 23641–23660 (2018).

16. X. Zhang, H. Ma, and J. Lucas, "Applications of chalcogenide glass bulks and fibres," J. Optoelectron. Adv. Mater. **5**, 1327–1333 (2003).

17. M. Anne, J. Keirsse, and V. Nazabal, "Chalcogenide glass optical waveguides for infrared biosensing," Sensors **9**(9), 7398–7411 (2009).

18. F. Starecki, F. Charpentier, J. Doualan, L. Quetel, K. Michel, R. Chahal, J. Troles, B. Bureau, A. Braud, P. Camy, V. Moizan, and V. Nazabel, "Mid-IR optical sensor for CO_2 detection based on fluorescence absorbance of Dy^{3+}: $Ga_5Ge_{20}Sb_{10}S_{65}$ fibers," Sens. Actuators, B **207**, 518–525 (2015).

19. J. A. Savage, P. J. Weber, and A. M. Pitt, "An assessment of Ge-Sb-Se glasses as 8 to 12 μm infrared transmitting glasses," J. Mater. Sci. **13**(4), 859–864 (1978).

20. A. R. Hilton and D. J. Hayes, "The interdependence of physical parameters for infrared transmitting glasses," J. Non-Cryst. Solids **17**(3), 339–348 (1975).

21. M. Frumar, H. Tichá, J. Klikorka and, and P. Tomiska, "Optical absorption in vitreous $GeSb_2Se_4$," J. Non-Cryst. Solids **13**(1), 173–178 (1973).

22. M. D. Rechtin, A. R. Hilton, and D. J. Hayes, "Infrared transmission in Ge-Sb-Se glasses," J. Electron. Mater. **4**(2), 347–362 (1975).

23. H. Parnell, D. Furniss, Z. Tang, N. C. Neate, T. M. Benson, and A. B. Seddon, "Compositional dependence of crystallization in Ge-Sb-Se glasses relevant to optical fiber making," J. Am. Ceram. Soc. **101**(1), 208–219 (2018).

24. R. Swanepoel, "Determining refractive index and thickness of thin films from wavelength measurements only," J. Opt. Soc. Am. A **2**(8), 1339–1343 (1985).

25. J. Orava, T. Kohoutek, T. Wagner, Z. Cerna, M. Vicek, L. Benes, B. Frumarova, and M. Frumar, "Optical and structural properties of Ge-Se bulk glasses and Ag-Ge-Se thin films," J. Non-Cryst. Solids **355**(37-42), 1951–1954 (2009).

26. Y. Wang, S. Qi, Z. Yang, R. Wang, A. Yang, and P. Lucas, "Composition dependences of refractive index and thermo-optic coefficient in Ge-As-Se chalcogenide glasses," J. Non-Cryst. Solids **459**, 88–93 (2017).

27. N. Carlie, N. Anheier, H. Qiao, B. Bernacki, M. Phillipes, L. Petit, J. Musgraves, and K. Richardson, "Measurement of the refractive index dispersion of As_2Se_3 bulk glass and thin films prior to and after laser irradiation and annealing using prism coupling in the near- and mid-infrared spectral range," Rev. Sci. Instrum. **82**(5), 053103 (2011).

28. J. M. Laniel, J. Menard, K. Turcotte, A. Villeneuve, R. Vallee, C. Lopez, and K. A. Richardson, "Refractive index measurements of planar chalcogenide thin film," J. Non-Cryst. Solids **328**(1-3), 183–191 (2003).

29. Y. Fang, L. Sójka, D. Jayasuriya, D. Furniss, Z. Q. Tang, C. Markos, S. Sujecki, A. B. Seddon, and T. M. Benson, "Characterising refractive index dispersion in chalcogenide glasses," *Proc. 18th International Conference on Transparent Optical Networks* (2016).

30. H. G. Dantanarayana, N. Abdel-Moneim, Z. Tang, L. Sojka, S. Sujecki, D. Furniss, A. B. Seddon, I. Kubat, O. Bang, and T. M. Benson, "Refractive index dispersion of chalcogenide glasses for ultra-high numerical-aperture fiber for mid-infrared supercontinuum generation," Opt. Mater. Express **4**(7), 1444–1455 (2014).

31. D. Poelman and P. Smet, "Methods for the determination of the optical constants of thin films from single transmission measurements: a critical review," J. Phys. D: Appl. Phys. **36**(15), 1850–1857 (2003).

32. Y. Fang, D. Jayasuriya, D. Furniss, Z. Q. Tang, C. Markos, S. Sujecki, A. B. Seddon, and T. M. Benson, "Determining the refractive index dispersion and thickness of hot-pressed chalcogenide thin films from an improved Swanepoel method," Opt. Quantum Electron. **49**(7), 237 (2017).

33. J. Senior, *Optical Fibre Communication: Principles and Practice*, 3rd edition (Pearson Education Limited, 2009).

34. D. Furniss and A. B. Seddon, "Thermal analysis of inorganic compound glasses and glass ceramics," in *Principles and Applications of Thermal Analysis*, Paul Gabbott, ed. (Blackwells, 2007).

35. D. C. Sati, A. Kovalskiy, R. Golovchak, and H. Jain, "Structure of $Sb_xGe_{40-x}Se_{60}$ glasses around 2.67 average coordination number," J. Non-Cryst. Solids **358**(2), 163–167 (2012).

36. P. Boolchand, P. Chen, and U. Vempati, "Intermediate Phase, structural variance and network demixing in chalcogenides: The usual case of group V sulphides," J. Non-Cryst. Solids **355**(37-42), 1773–1785 (2009).

37. P. W. France, M. G. Drexhage, J. M. Parker, M. W. Moore, S. F. Carter, and J. V. Wright, *Fluoride Glass Optical Fibres* (Blackie, 1990).

38. L. Petit, N. Carlie, F. Adamietz, M. Couzi, V. Rodriguez, and K. C. Richardson, "Correlation between physical, optical and structural properties of sulfide glasses in the system Ge–Sb–S," Mater. Chem. Phys. **97**(1), 64–70 (2006).

39. S. M. El-Sayed, "Far-infrared studies of the amorphous $Sb_xGe_{28-x}Se_{72}$ glass semiconductor," Semicond. Sci. Technol. **18**(4), 337–341 (2003).

40. G. P. Agrawal, *Nonlinear Fiber Optics*, 5th edition (Academic Press, 2013).

41. Amorphous Materials Inc, "AMTIR-2 Information" (consulted December 2018).

42. J. M. Dudley and J. R. Taylor, *Supercontinuum Generation in Optical Fibers* (Cambridge University Press, 2010).